Verification of a Mathematical Model for Aerosol Nitrate and Nitric Acid Formation, and Its Use for Control Measure Evaluation

Armistead G. Russell[+] and Glen R. Cass[x]

Environmental Quality Laboratory 201-40
California Institute of Technology
Pasadena, California 91125

ABSTRACT

A mathematical model for the formation of atmospheric nitric acid and aerosol nitrate has been developed and employed to study the effect of emission controls. Based on a Lagrangian formulation of the atmospheric diffusion equation, the model computes nitric acid concentrations from a description of daytime photochemical reactions and nighttime reactions involving NO_3 and N_2O_5. Ammonium nitrate formation is computed at thermodynamic equilibrium between HNO_3 and NH_3, and heterogeneous reactions between HNO_3 and preexisting aerosol are considered. The accuracy of the air quality model's predictions is verified by comparison to O_3, NO_2, HNO_3, NH_3, aerosol nitrate, and PAN measurements made for this purpose in California's South Coast Air Basin during the period of 30-31 August 1982.

Examination of emission control alternatives shows that reduction in NO_x emissions yields a nearly proportional decrease in total inorganic nitrate levels (HNO_3 + aerosol nitrates). Reduction in NH_3 emissions suppresses aerosol nitrate formation, resulting in higher HNO_3 levels. Control of organic species emissions by the amounts expected in Los Angeles in future years causes a partial shift away from PAN formation toward greater production of HNO_3. Emission control strategies can be formulated that include a combination of controls on NO_x, organic gases, and NH_3 emissions that will achieve a greater reduction in HNO_3, aerosol nitrate, and O_3 levels than a strategy predicated on control of only a single precursor species.

Key word index: ammonia, dinitrogen pentoxide (N_2O_5), hydrocarbons, nitrate aerosol, nitrate radical (NO_3), nitric acid, nitrogen dioxide, ozone, peroxyacetyl nitrate, photochemical modeling, emission control

+ Department of Mechanical Engineering

x Environmental Engineering Science Department

1. Introduction

Anthropogenic emissions of NO_x and reactive organic gases (ROG) are the recognized precursors for a number of pollutants found in the atmosphere including O_3, NO_2, HNO_3, and aerosol nitrate (AN). Emission control measures are being taken to reduce the formation of O_3 and NO_2 in areas with excessive concentrations. These control programs are expensive, and the most effective strategies to reduce O_3 and NO_2 concentrations (Pitts et al., 1983; Chock et al., 1981, 1983; Glasson, 1981, 1983) are still in question. A key problem faced when selecting between alternative control programs is that the decisions made will also affect the concentrations of a number of currently unregulated but potentially damaging co-pollutants, in particular HNO_3 and AN. HNO_3 production results in deposition of strong acids at the earth's surface. HNO_3 also reacts with NH_3 and preexisting particulate matter in the atmosphere to produce fine AN which is very effective in reducing visibility.

The purpose of the present study is to develop and test engineering methods for predicting the effect of ROG, NO_x, and NH_3 control programs on atmospheric HNO_3, O_3, and AN concentrations. A photochemical trajectory model that predicts O_3, NO_2, total inorganic nitrate (TN), AN, HNO_3, NH_3, and PAN concentrations from emissions data is tested for its ability to reproduce field experimental data. Following this evaluation, the air quality model is used to determine the effect that reducing the emissions of ROG, NO_x, and NH_3 has on O_3, PAN, HNO_3, NH_3, and AN concentrations. Example calculations are presented for Rubidoux, near Riverside, CA, which experiences some of the most serious nitrate-induced fine particulate loading and visibility problems in the U.S.

2. Model Description

Results presented in this paper were obtained using a Lagrangian

trajectory formulation of the atmospheric diffusion equation that describes atmospheric chemical reactions, turbulent vertical diffusion, horizontal advective transport, and ground level pollutant deposition. Within the chemical mechanism the concentration of ammonium nitrate aerosol is computed to be at thermodynamic equilibrium with NH_3 and HNO_3 vapor, and where noted, the heterogeneous formation of AN from the reaction of HNO_3 with preexisting aerosol is treated. Except for the following specific details, a complete description of the gas phase model appears elsewhere (Russell et al., 1983, 1985), and it will not be described further here.

Reaction 58, describing the interaction between preexisting aerosol and HNO_3, has been added to the previously described version of this model in order to simulate the stripping of atmospheric HNO_3 by certain aerosols, such as sea salt,

$$\text{SINK} + HNO_3 \xrightarrow{58} \text{BAN}$$

where SINK is that portion of the aerosol material available to react with HNO_3 and BAN is irreversibly Bound Aerosol Nitrate. This is a generalized reaction that includes a variety of specific chemical reactions, such as the displacement reaction

$$NaCl(s \text{ or } aq) + HNO_3(g) \rightarrow NaNO_3(s \text{ or } aq) + HCl(g)$$

which is thermodynamically favorable, and is suggested by the excess of Na^+ ions in comparison to the Cl^- ions in many atmospheric aerosol samples (Russell and Cass, 1984; Duce, 1969; Martens et al., 1973). The rate constant for this reaction is derived from kinetic theory for the bombardment of the aerosol surface by HNO_3 vapor. Aerosol surface area per unit mass is computed from the size distribution of Larson et al. (1984), which was obtained on a moderately smoggy August day in California's South Coast Air Basin (SoCAB).

Collision efficiencies for the reactions between gases and atmospheric aerosol surfaces vary with aerosol surface characteristics and composition and are not known for all the relevant combinations of reactive gases and aerosols. Baldwin and Golden (1979) measured a value of 2.4×10^{-4} as the lower bound on the collision efficiency of HNO_3 with an H_2SO_4 surface. With this in mind, a collision efficiency of 0.001 was assumed for the reaction of HNO_3 vapor with the SINK aerosol surface.

In this study, the height of the air column modeled is 1000 m, divided into 10 cells with vertical dimensions of 30, 50, 70, five 100, 150 and 200 m. The emissions inventory, meteorological fields, and terrain characteristics are developed on a grid system containing 5 km by 5 km cells, so the horizontal dimensions of the air parcels studied are set to the same size as a single grid cell.

3. Model Evaluation Data Base

3.1 Pollutant Concentrations

Model evaluation tests will be conducted using a number of air parcel trajectories that cross the SoCAB (Fig. 1) on 30-31 August 1982. During this 2-day period an experiment was conducted to acquire a set of data for use in verifying this type of photochemical air quality model (Russell and Cass, 1984). That set of experimental data includes observations on AN, sulfate, ammonium, and other ionic species concentrations, as well as gas phase NH_3, HNO_3, and PAN levels. Gas phase concentrations of total hydrocarbons (THC), CO, NO, NO_x, and O_3 for this time period were obtained from South Coast Air Quality Management District (SCAQMD) and California Air Resources Board (CARB) monitoring stations that are colocated with the aerosol monitoring sites. PAN concentrations were measured at the University of California, Riverside, (UCR) and at Caltech in Pasadena, CA.

3.2 Hourly Meteorological Data

Wind fields for the 2-day period of interest were obtained using measured wind velocities at 39 sites in the SoCAB. These wind data were interpolated over the 80 by 30 grid of 25 km^2 cells superimposed over the air basin using the r^{-2} weighting method detailed by Goodin et al. (1979). Air parcel trajectories were calculated from these wind fields using 10-min time steps. 1-h average temperature and relative humidity fields were obtained by interpolation between the 29 and 18 locations at which these parameters are measured, respectively. 1-h average mixing depth fields were obtained from the measured vertical atmospheric temperature profiles available at 8 locations. Solar radiation levels measured at downtown Los Angeles, Pasadena, and Upland were used to set the photolysis rate constants within the chemical mechanism.

3.3 Emissions

NO_x, total hydrocarbon (THC), and CO emissions into the air parcels modeled are calculated from a 1982 forecast emission inventory for the SoCAB provided by the California Air Resources Board (Ranzieri, 1983, 1984). The inventory details the emissions, by species, from over 2600 source categories distributed spatially and temporally over the basin. Hourly emission rates are given for over 200 organic species, NO, NO_2, and CO for each of the 5 km X 5 km grid cells throughout the SoCAB. A summary of the daily totals of the emissions from mobile and stationary sources is given in Table 1. The spatial distributions of the THC, NO_x, and CO emissions are shown in Figure 2. Emission rates given for the individual organic gas species are lumped into the 6 organic classes compatible with the model used in this study.

The NH_3 emissions inventory for 1982 used in this study was developed by updating the 1974 emissions inventory previously described by Cass et al. (1982) and Russell et al. (1983). Total NH_3 emissions by source category are shown in Table 2, and the spatial distribution of NH_3 emissions is given in Figure 2. Variables that affect NH_3 emissions from animal waste decomposition have been investigated by Muck and Steenhuis (1982) and Steenhuis et al. (1982). Based on their work, the diurnal variation of the NH_3 release rate from animal waste decomposition is assumed to depend on temperature and wind velocity, such that:

$$E_i \propto 2.36^{\left(\frac{T_i-273}{10}\right)} V_i^{0.8} A \qquad (1)$$

and

$$A = \sum_{i=1}^{24} E_i \qquad (2)$$

where E_i is the hourly emission rate in the grid cell at hour i from animal waste decomposition, A is the daily total emission rate of NH_3 from animal waste in the grid cell, T_i is the absolute temperature in °K, and V_i is the wind velocity in m s^{-1} at hour i. A minimum wind velocity of 0.1 m s^{-1} is assumed.

3.4 Initial Conditions

Surface level initial conditions for trajectories ending at Rubidoux were based on the concentration fields constructed by spatial interpolation of the measured concentrations. Those concentration fields start with the Pacific Ocean background values (in ppb: O_3, 40; NO_2, 10; NO, 10; CO, 100; HNO_3, 1; NH_3, 1; THC, 1000) at the western edge of the grid and rise to match the on-land data at the near coastal monitoring sites established during the field experiment. Initial upper level pollutant concentrations over the ocean

were set to (in ppb): O_3, 40; NO, 0.0; NO_2, 1.0; CO, 500; HNO_3, 1.0; NH_3, 1.0; and THC, 500. Initial NH_4NO_3 concentrations over the ocean were set to 3.25 $\mu g\ m^{-3}$ (the NO_3^- equivalent of 1 ppb HNO_3).

Atmospheric THC measurements taken by the SCAQMD are reported on a ppm C atoms basis and are not speciated into the many different organic gases actually present. The initial conditions for each of the 6 hydrocarbon (HC) classes employed by the trajectory model are found by splitting the measured THC values into the 6 classes using the set of splitting factors given in Table 3. These factors were derived from the measurements taken by Grosjean and Fung (1984) of the speciated HC composition of Los Angeles air, averaged over a number of sampling periods.

4. Model Evaluation for 30-31 August 1982

The ability to accurately predict O_3 and NO_2 concentrations usually is the most stringent test used to evaluate a gas phase photochemical model. In this study, the ability to calculate total inorganic nitrate (TN), HNO_3, NH_3, AN, and PAN will be tested in addition to O_3 and NO_2.

Progress towards model verification for a few of these co-pollutants was reported by Russell et al. (1983), when an earlier version of this model was tested using nitrate ion, ammonium ion, and NH_3 gas concentration data available for a short period on 28 June 1974. Model verification data used during that study were limited, and because the AN samples were collected on glass fiber filters, questions of artifact nitrate formation cloud the assessment of data quality. In this section a much more extensive model evaluation effort is carried out for the 2-day period of 30-31 August 1982.

Two sets of trajectories are studied in this evaluation: a forward trajectory starting at Long Beach and ending near Rubidoux, and a set of trajectories ending at Rubidoux throughout 31 August 1982. Rubidoux is in the

eastern portion of the SoCAB, downwind of the Los Angeles metropolitan area, and is affected by the reaction products formed in the atmosphere downwind of a major city. Long-term air quality data taken throughout the SoCAB during 1982 (Gray et al., 1985) show that Rubidoux is the monitoring site with the highest AN levels, as has been the case historically. The Rubidoux-Riverside area also experienced the highest total nitrate levels observed during the 30-31 August 1982 period studied here and had the highest measured O_3 concentrations during this 2-day interval (230-260 ppb). As such, these trajectories serve as ideal candidates for model verification tests and can be used to show the effect of emission control strategies on pollutant concentrations. Further model verification also was conducted using the data from the Upland monitoring site, and the results are found in Russell (1985).

4.1 Long Beach Forward Trajectory

During a previous examination of the data from the 1982 field experiment (Russell and Cass, 1984), an air parcel trajectory was identified that started in the morning at the Long Beach sampling site at the time of the AN peak at that location, passed just north of the Anaheim measurement station in the afternoon, and in the evening terminated close to the Rubidoux site at the time of the AN peak in the Riverside area. This single trajectory provides an ideal opportunity for use in part of the model evaluation effort because the contents of the air parcel are well defined at several locations along its path. Likewise the initial conditions are established using measured pollutant concentrations, minimizing the uncertainty added from interpolating data.

Two distinct calculation schemes were tested against the measurements taken along the Long Beach to Rubidoux trajectory just discussed. In the first calculation, Case 1, AN was assumed to be formed only by the reaction

between NH_3 and HNO_3. In the second test, Case 2, AN formation proceeded by the reaction of HNO_3 with NH_3, and by the irreversible reaction of HNO_3 with preexisting aerosol (reaction 58, described previously). Use of reaction 58 requires that emissions along the trajectory be specified for the aerosol materials that react readily with HNO_3. The emission rate of SINK aerosol available to react with HNO_3 was set at a constant rate, such that the total unreacted SINK aerosol plus the cations associated with BAN at the end of the trajectory was approximately equal to the sum of the Na, Ca, K, and Mg concentrations measured when the trajectory reached Rubidoux. Actual emission rates of these species as a function of location are unknown.

Results of the Long Beach to Rubidoux forward trajectory calculations are shown in Table 4, along with the measured pollutant concentrations, at 1400 and 1800 PDT, 31 August 1982. The trajectory passed nearest to Anaheim at 1400 PDT, and the measured HNO_3, NH_3, AN, and TN concentrations at that time are from that station. Measured O_3 and NO_2 values at 1400 are available from a number of monitoring sites in the area, and the O_3 and NO_2 values shown are an average of the values at the 3 stations nearest to the air parcel's position at that time. As the trajectory passed near Anaheim at 1400, the O_3 prediction very nearly equals the observed average, well within the uncertainty in the observed concentrations. The predicted NO_2 concentration, corrected to include those species that interfere with the measurement devices (Winer et al., 1974), is slightly lower than the observed. In both Cases 1 and 2, the predicted HNO_3 level is between the values measured for the sampling periods straddling 1400 PDT. The AN predicted for Case 1 is between the measured concentrations, while the amount predicted in Case 2 is slightly greater than the observed values. In both cases the predicted NH_3 matches the 2 measured values to within the measurement uncertainties.

Farther downwind, at 1800 PDT, the trajectory path calculation showed that the air parcel was 3 km southwest of the Rubidoux sampling site and about 8 km west of the Riverside (UCR) site. Ozone, predicted to be 152 ppb, is equal within the reporting uncertainty of 10 ppb to that measured in Riverside and is slightly greater than that measured at Rubidoux. Again the NO_2 predictions are slightly below the measured values. In this case, the trajectory arrival at Rubidoux again straddles 2 measurement periods for HNO_3, NO_3^-, and NH_3, while at the UCR site the 1800 arrival falls within a single sampling interval. In both Cases 1 and 2, the predicted concentrations of HNO_3, AN, and TN fall within the range of the observations at Rubidoux and Riverside. The predicted NH_3 concentration resulting from the Case 2 calculation also lies within the measured range. While the NH_3 concentration prediction for Case 1 may appear slightly lower than that observed at UCR, the circa 5 ppb NH_3 deficit is still within the experimental uncertainty of the NH_3 concentration measured at UCR at that time (Russell and Cass, 1984).

PAN also was measured at the UCR site, and as seen in Table 4, the model closely predicts the observed PAN concentration, which peaked at that time. From the results shown in Table 4, it is concluded that the trajectory model is capable of predicting the downwind concentrations of the secondary pollutants of interest in the Riverside area at the time of arrival of the peak nitrate concentrations, given measured initial conditions at Long Beach.

4.2 Trajectories Ending at Rubidoux

While the Long Beach to Rubidoux trajectory calculation adds to confidence in the model's capability, it is unrealistic to expect that high quality data on initial conditions always will be available for arbitrarily selected trajectories. Likewise, the upper level pollutant concentrations needed to initialize the model are seldom, if ever, known. Upper level

initial conditions must be estimated from ground level measurements, while pollutants stored aloft may have been affected by chemical processes not evident at the ground. This is especially true in the early morning because of the markedly decreased vertical mixing overnight that traps fresh emissions near the ground and isolates portions of the upper air column from nighttime emissions and from deposition. In this case the ground level portion of the air mass may be heavily burdened by NO and NO_2, while in the upper levels of the atmosphere nighttime chemical reactions can convert almost all of the NO and NO_2 to HNO_3 (Russell et al., 1985). If this situation is not taken into account, initial conditions based on ground level observations could be specified that are inconsistent with actual pollutant concentrations several hundred m above the ground.

An alternative method for initializing trajectories was examined. Air parcels arriving at Rubidoux throughout the day of 31 August were followed backward to midnight at the end of 29 August. In that case all the trajectories begin over the ocean upwind of the city and end between 24 and 47 h later at the Rubidoux monitoring site. Use of the longer, 2-day trajectories has 3 major advantages. First, starting more than 24 h before the arrival of the trajectory allows sufficient time for most of the reactive pollutants present due to initial conditions to be depleted from the system both by ground level deposition and by chemical reactions that form products less crucial to the formation of photochemical oxidants. Secondly, starting the air parcel at a relatively clean background location over the ocean minimizes the effect of initial conditions and the uncertainty in the outcome arising from their specification. Thus, predicted concentrations at the end of the trajectory are primarily a function of the emissions along the trajectory, not of initial conditions, and the mass of each species in the air

parcel at the start of 31 August is consistent with the known emissions, meteorology, and chemistry of 30 August. Finally, this procedure enhances the usefulness of subsequent control strategy calculations because predicted concentrations are dominated by emissions along the trajectory that can be attributed to particular air pollution sources rather than being heavily influenced by initial conditions that are not readily assigned to their source. This is a more demanding test of a model and the associated emissions inventory than is the case when using shorter trajectories in which initial conditions play a major, if not dominating, role.

In an effort to determine the importance of uncertainties in the initial conditions, a test was performed in which the initial concentrations established over the ocean were first doubled and then halved for the trajectory arriving at Rubidoux at 1600 PDT. This trajectory displayed the greatest predicted nitrate loading and second highest O_3 concentration among the trajectories terminating at Rubidoux. The predicted TN concentrations at Rubidoux at 1600 PDT for the base case, for the case with the initial conditions doubled, and for the case with initial concentrations cut in half were 18.2, 15.5, and 20.6 ppb, respectively. The O_3 concentrations averaged over the last 1-h of travel along that trajectory were 185, 195, and 176 ppb, respectively. This test shows that initial conditions play a very small role in determining predicted pollutant concentrations for the multi-day trajectories studied here. On the other hand, if the emissions are set to zero along this same trajectory, the total inorganic nitrate predicted at Rubidoux falls to only 1.6 ppb, and O_3 falls to 38 ppb. Thus, the predicted pollutant levels are almost solely a function of emissions within the urban area when a reasonable set of initial conditions starting over the ocean is used.

Next the air quality model's ability to reproduce the time history of pollutant concentrations at Rubidoux given trajectories that originate over the ocean was examined. Again the model was evaluated in 2 modes: with and without the addition of aerosol that can irreversibly react with HNO_3 to form AN.

Plots of the pollutant concentrations predicted at Rubidoux for 31 August without the emission of SINK aerosol along the trajectories are compared to measured values in Figures 3 through 8. Ozone and NO_2 concentrations averaged over the last 1-h of travel are shown in Figures 3 and 4. Trajectories arriving at Rubidoux on the hour were used to estimate 2-h average concentrations when needed for comparison to measured values (2-h average weighted ¼ start hour, ½ midpoint, ¼ end hour). Predicted 2-h average TN concentrations are shown, with the measured values, in Figure 5, HNO_3 in Figure 6, AN in Figure 7, and NH_3 in Figure 8.

A plot of the predicted and observed concentrations of O_3 and NO_2 throughout 31 August at Rubidoux shows that the model predictions are in good agreement with the measured species concentrations. Figure 5 shows the comparison of averaged predicted and observed TN. The model predicts the trends and, approximately, the 2-h average concentrations. The peak predicted TN, 38 $\mu g\ m^{-3}$ (as NO_3^-), is only slightly less than the peak measured, 43 $\mu g\ m^{-3}$, which is considered close given measurement and model input uncertainties. The predicted 24-h average TN is 19 $\mu g\ m^{-3}$, against a measured 18 $\mu g\ m^{-3}$.

Having shown that the predicted and measured TN agree well, the question of apportioning the TN between the gas and aerosol phases arises. This is sensitive to the temperature, humidity, and NH_3 concentration (Russell et al., 1983), and to the presence of other aerosol constituents (Hildemann

et al., 1984). In the first case studied here, pure NH_4NO_3 is assumed to be the only AN species formed. Most of the inorganic nitrate is predicted to be found in the aerosol phase, not the gas phase, and the measurements confirm that prediction (Fig. 6). The measured and predicted 24-h average AN concentrations were 13 and 16 $\mu g\ m^{-3}$, respectively (Fig. 7). Measured gas phase HNO_3 levels in this case exceed observed values throughout the day (Fig. 6), but the absolute magnitude of this discrepancy is very small. The measured 24-h average HNO_3 was 1.9 ppb compared to the predicted 1.1 ppb. Measurement uncertainties on the HNO_3 values are approximately 0.4 ppb (one standard error).

A plot comparing the NH_3 concentrations, Figure 8, indicates that throughout much of the day the predictions agree remarkably well with the measurements considering that the NH_3 emission inventory and model used here represent the first test of a procedure for calculating atmospheric NH_3 levels. The 24-h average NH_3 measured was 51 ppb, compared to the predicted 61 ppb.

In the trajectories terminating at Rubidoux, most of the NH_3 emissions are due to livestock operations, which determine the very tall spike in the NH_3 emission inventory (Fig. 2) located immediately upwind of Rubidoux. The major peak in the NH_3 emission inventory is so sharp that a slight perturbation in the calculated path of an air parcel can create a noticeable difference in the predicted NH_3 concentrations. Also, knowledge of the diurnal emission pattern for livestock waste decomposition and the exact spatial distribution of the animals during the August 1982 experiment could be improved. As a result, NH_3 concentrations cannot be predicted with the same precision as other pollutant concentrations, even though the source of the NH_3 emissions has been identified with reasonable certainty.

In view of the sensitivity of the model's nitrate predictions to NH_3 concentration and temperature and of the uncertainty in the NH_3 emissions from the large sources just upwind of Rubidoux, a second set of calculations was performed in which TN concentrations predicted by the model were apportioned between gas phase HNO_3 and aerosol NH_4NO_3 using the ambient NH_3 concentrations and temperatures measured at Rubidoux. The temperatures at Rubidoux used in the previous modeling calculations were obtained from filtered, interpolated temperature field values calculated for the center of each grid cell and need not equal the measured temperatures at Rubidoux exactly. Using the measured ambient temperature and NH_3 concentration to partition the nitrate at the trajectory endpoint improved the model predictions from those shown in Figure 7 to those shown in Figure 9. Thus, given the ability to predict more precisely the NH_3 concentrations and using actual measured temperatures, the model can accurately partition the inorganic nitrate at Rubidoux between the vapor and aerosol phases. This calculation also decreases the predicted 24-h average AN from 16 $\mu g\ m^{-3}$ to 12 $\mu g\ m^{-3}$, bracketing the measured value of 13 $\mu g\ m^{-3}$.

Next the emissions of SINK aerosol were added along each trajectory at a constant rate needed to approximately match the total non-ammonium cationic material seen to arrive at Rubidoux. The entire set of multi-day trajectory calculations beginning over the ocean was repeated with HNO_3 allowed to react with SINK aerosol by reaction 58, and again using the measured ambient temperature and NH_3 concentration at Rubidoux to apportion TN between HNO_3 and the aerosol phase. This change in assumptions tends to increase the AN and TN concentrations predicted, though in this case the effect is small. As seen in Figure 10, the 24-h average AN increases to 18.4 $\mu g\ m^{-3}$, of which 84% is ammonium nitrate and the remaining 16% is BAN. The model predicts the

coexistence of ammonium nitrate, BAN, HNO_3, NH_3 and unreacted aerosol SINK, indicating that the consumption of aerosol SINK is kinetically limited. Given more time, or if the collision efficiency for HNO_3 on SINK aerosol is much higher than $\alpha = 0.001$, then the aerosol has the capacity to strip a large fraction, if not all, of the HNO_3 from the atmosphere.

In this study, results from shorter (single day) and longer (multi-day) trajectories have been used to evaluate the model's performance. In both cases the model has performed well. Some uncertainty in the air parcel path is added to the analysis when trajectory paths are calculated over multi-day periods, as discussed in Russell (1985). However, this is the only way to decrease the uncertainties that would otherwise arise from misspecifying initial conditions and to accurately show the effects that changing pollutant emissions would have on the resulting concentrations. If initial conditions dominate or greatly affect the predicted concentrations, a change in emissions within the model may have little effect on model predictions, or in some cases could produce predictions that move in a direction opposite to reality. An example of the latter case could arise if initial conditions placed an excessive amount of NO_x in the air parcel as it starts in the morning. In this case increasing NO emissions further could decrease the peak O_3 concentration, while if the correct initial NO_x concentrations were used, then the atmosphere might be sufficiently starved for NO_x that further NO_x emissions would increase predicted O_3 levels.

The use of multi-day trajectories could suffer from the effects of vertical wind shear at night. On this particular occasion it appears that these effects were small. Upper level wind data were collected at a number of sites. At Point Mugu where the early morning winds were measured at 419 PDT, the winds varied little in direction (less than 10°) with height. Upper level

velocities also were low, less than 2.5 m s^{-1}, to well above the height of the modeling region. In the eastern portion of the basin, the early morning measurement taken at 300 PDT showed that the difference in velocity between the ground and levels up to 188 m was less than 1 m s^{-1} with direction varying no more than 25°. 188 m is greater than the depth of the early morning mixed layer trapping the pollutants emitted at ground level.

The above discussion, along with the successful model evaluation results, argues that multi-day trajectories can, and should, be used for testing the effects of emission control measures.

5. Evaluation of Control Strategies for HNO_3 and Aerosol Nitrate Abatement

To help guide researchers and public agencies toward an optimal control strategy, the effects of a number of simple candidate control strategies are simulated and the results will now be discussed. The study is directed primarily towards developing strategies that will reduce AN and HNO_3 concentrations in the atmosphere, but the effect on pollutants other than HNO_3 and AN also will be detailed. As discussed above, because of the high nitrate and O_3 concentrations the Rubidoux trajectories were chosen for emission control measure evaluation.

Choice of the first set of control measures examined was motivated by the 1982 Air Quality Management Plan (AQMP) for the SoCAB (SCAQMD and Southern California Association of Governments, 1982). The AQMP outlines control measures that will be used to decrease NO_x emissions by about 23% and ROG by about 34% between the years 1979 and 1987, or about a 20% and 30% decrease, respectively, below the 1982 estimated emissions inventory used in the present study. For the purpose of this study, these reductions will be applied homogeneously over the air basin and will be applied equally to emissions of each of the lumped organic species. In a more detailed analysis, the original

emissions inventory could be modified to reflect the specific reductions in each source category. This would result in a less spatially homogeneous reduction and could change the relative chemical composition of the organic emissions.

Table 5 shows the effects on the inorganic nitrate species of different combinations of emission reductions applied to the multi-day trajectories ending at Rubidoux. Pollutant emissions into these trajectories as they actually occurred on 31 August 1982 will be referred to as the base case emissions, and the observed NH_3 concentration and temperature at Rubidoux are used to apportion total inorganic nitrate between HNO_3 and AN. Results in Table 5 are for the case without the addition of SINK aerosol to react with HNO_3. The effect of including the addition of SINK via reaction 58 on various control measures will be discussed later. Predicted maximum 2-h average AN, 24-h average AN, 24-h average TN, and maximum 2-h HNO_3 are given in each case for comparison.

A 20% decrease in the NO_x emissions alone relative to the base case decreases the predicted maximum AN 40%, and the 24-h average AN value decreases 27%. TN decreases about 18%, or by about the same percentage as the decrease in NO_x emissions. Less change is noted in the predicted HNO_3. This occurs because HNO_3 concentrations are largely governed by the NH_4NO_3 equilibrium dissociation constant and the ambient NH_3 concentrations. The excess of NH_3 tends to allow only a small amount of HNO_3 in the gas phase while the rest of the inorganic nitrate is transferred into the aerosol phase. Elsewhere in the air basin, NH_3 levels are much lower and a change in TN would be reflected more readily in a change in HNO_3 levels.

Decreasing the organic gas emissions results in an increase in AN, TN, and HNO_3. At first glance this is a slightly discouraging result. Careful

examination shows that this increase in inorganic nitrate is primarily due to the oxidized nitrogen being displaced from PAN into inorganic nitrate species. Under some circumstances this trade-off between organic and inorganic nitrate species formation might be deliberately manipulated in order to achieve a desired balance between TN and PAN. Decreasing organic gas emissions also may decrease the formation of other potentially harmful organic and nitrated organic compounds not studied here.

Reducing the NO_x and organic emissions has a beneficial effect on reducing the O_3 levels (Table 6). Note that a 20% decrease in NO_x emissions from the base case decreases the maximum O_3 at Rubidoux by more than a 30% decrease in organic emissions for the particular event examined here. This finding differs from the results of some previous studies. Possible reasons for these differences are discussed later.

Just before arriving at Rubidoux, the trajectories pass over a number of farming and animal husbandry operations, resulting in the high observed NH_3 concentrations. One possible control strategy for reducing the AN concentrations could be predicated on relocating these large NH_3 sources. The same result may be achieved indirectly as urban sprawl pushes farming operations further away from the center of the SoCAB. To simulate this possibility, NH_3 emissions from farm-oriented operations (due to livestock waste and fertilizer used for agricultural purposes) were removed from the inventory. The same sets of trajectory calculations used in the previous control measure evaluation study were repeated except that the NH_3 emissions were reduced. These results are given in Table 5. The 24-h average NH_3 concentration at Rubidoux decreased from the base case value of 51.0 ppb down to 4.3 ppb when farm-related activities were eliminated. Decreasing the NH_3 has a tremendous effect on the ammonium nitrate and HNO_3 predictions. With

farm-related NH_3 emissions removed, only 2.8 μg m^{-3} of nitrate is found in the aerosol phase, compared to 13.3 μg m^{-3} of HNO_3 gas, a reversal of the base case. Reducing NH_3 to control AN formation results in an increase in HNO_3 and the problems associated with HNO_3. Thus, the advantages and disadvantages of this avenue of control must be weighed before any action is taken.

If SINK aerosol is present that can react with HNO_3 to produce AN, reducing the NH_3 emissions does not lead to as large a decrease in AN as was predicted above for the case of a pure NH_3, HNO_3 and NH_4NO_3 system. Increased HNO_3 concentrations that result from NH_3 removal lead to more BAN being formed due to reaction 58. As shown in Table 7, the 24-h average AN drops from 13.8 μg m^{-3} with the base case level of NH_3 emissions to 8.3 μg m^{-3} for the reduced NH_3 case--not as drastic a reduction as when no SINK is included in the calculations.

Further reduction of NO_x emissions beyond the 20% anticipated by the AQMP was examined. TN concentrations were seen to decline in almost direct proportion to changes in NO_x emissions. Reducing NO_x emissions by 20, 40, 60, and 80% resulted in a decrease in TN of 18, 45, 64, and 78%, respectively, at Rubidoux. A similar, almost linear dependence, between HNO_3 formation and NO_x input was found by Spicer (1983) in smog chamber experiments. Returning to the present study, AN decreased at a slightly greater rate than TN: 27, 58, 78, and 90% for the four levels of decreased NO_x emissions defined above. Maximum O_3 concentrations predicted at Rubidoux also declined as NO_x emissions were decreased. During the present study, a 60% reduction in NO_x emissions would have been sufficient to meet the federal O_3 standard along the trajectories ending at Rubidoux.

In some previous modeling studies investigators have found that, contrary to the case examined here, lowering NO_x emissions can increase O_3

concentrations. There are obvious reasons that could account for the different findings and some more subtle reasons, too.

First it is well known that depending on the HC to NO_x ratio in an air parcel, NO_x control can either increase or decrease O_3 concentrations. A different mix of organic gas and NO_x emissions resulting from different trajectory paths and the fact that emission inventories for different years have been used could account for part of the difference in the O_3 response to NO_x emission changes. Along the same lines, some investigators have examined the effect of a further decrease in NO_x emissions only after a large decrease in ROG emissions from mobile sources was imposed. This results in a larger reduction in total ROG emissions than studied here and also a different organic gas emission composition. Also, there are inherent differences in the many models that have been used in the past. More subtle causes for the differences in the outcomes of the calculations may well lie in the way that the trajectories are initialized. If shorter trajectories are used, as has been customary in previous studies, then the choice of initial conditions can play a very large role in determining the results. Application of emission controls will affect those initial conditions, but a great deal of uncertainty surrounds the question of estimating the effect of emission controls on initial conditions for short trajectories that start over land within the air basin. If in previous modeling studies the concentrations of NO and NO_2 in the upper levels of a model at the start of the trajectory were based on ground level observations in the morning, then those NO and NO_2 levels may have been estimated to be much higher than reasonably could be expected. Nighttime reactions between NO_2 and O_3 could convert almost all the NO_2 present aloft at night to HNO_3 by sunrise the next morning (Russell et al., 1985). Organic gases, however, can persist aloft at night because little or

no photolysis takes place and because OH radical concentrations are greatly reduced at night. As the mixing depth increases the next day, the air entrained downward from aloft is comparatively lean in NO and NO_2, and, as a result, fresh NO_x emissions are required to promote the formation of O_3.

This study concludes that reducing NO_x emissions will result in lower AN, HNO_3, PAN, and NO_2 concentrations. Lowering NO_x and ROG emissions also may decrease the formation of other nitrogenous organic compounds, certain of which are mutagenic and carcinogenic (Ohgaki et al., 1982). For the case considered here, NO_x control, independently or combined with ROG control, also assisted in controlling O_3 at Rubidoux, although it is not clear that that result is true in general at other times and locations.

6. Conclusions

The predictions of a trajectory model describing the photochemical dynamics of O_3, NO_2, HNO_3, PAN, and AN were compared to field measurements. Predicted O_3 and NO_2 concentrations closely followed the measured concentrations. Predicted TN concentrations at Rubidoux were very close to those measured at that site, often matching observations to within experimental error. The ability to closely account for the origin of measured O_3, NO_2, and TN concentrations is one of the most severe tests of a gas phase photochemical model. Model predictions of the apportionment of TN between the aerosol and gas phases compare satisfactorily to the observations through much of the day, although on the average the model underpredicts the HNO_3 concentrations by a fraction of a ppb. This could be due to a number of reasons. Among the more likely reasons are inaccuracies in the interpolated temperature fields and uncertainties in the NH_3 emissions inventory. When the observed ambient NH_3 concentrations and temperature are used to apportion the TN between the gas and aerosol phases, the AN predictions match observations

very well. In spite of the uncertainties, the predicted NH_3 levels are close to the observed values, averaging slightly greater than observed, indicating that the inventory does not differ greatly from the actual emissions.

Control strategy tests indicate that reductions in NO_x emissions would result in nearly proportional reductions in TN formation and slightly greater than proportional reductions in AN. For the cases studied, O_3 concentrations also declined as the NO_x emissions were reduced. Decreasing ROG emissions also lowered O_3 concentrations and decreased organic nitrate (PAN) concentrations, though at the expense of increasing inorganic nitrate formation.

AN formation at Rubidoux would be greatly decreased if NH_3 emissions from farm-related operations were suppressed. However, a corresponding increase in HNO_3 concentrations would be expected to accompany this approach to AN control. Combined emission control strategies can be formulated that include a combination of controls on ROG, NO_x, and NH_3 emissions that will achieve a greater control of AN and HNO_3 levels than a strategy predicated on control of only a single precursor species.

Acknowledgements

This work was supported by the California Air Resources Board under Agreement A2-150-32.

References

Baldwin A.C. and Golden D.M. (1979) Heterogeneous atmospheric reactions: Sulfuric acid aerosols as tropospheric sinks. Science 206, 562-563.

Cass G.R., Gharib S., Peterson M. and Tilden J.W. (1982) The origin of ammonia emissions to the atmosphere in an urban area. Open File Report 82-6, Environmental Quality Laboratory, California Institute of Technology, Pasadena, CA.

Chock D.P., Dunker A.M., Kumar S. and Sloane C.S. (1981) Effect of NO_x emission rates on smog formation in the California South Coast Air Basin. Envir. Sci. Technol. 15, 933-939.

Chock D.P., Dunker A.M., Kumar S. and Sloane C.S. (1983) Reply to Comment on "Effect of nitrogen oxide emissions in metropolitan regions," "Effect of NO_x emission rates on smog formation in the California South Coast Air Basin", and "Effect of hydrocarbon and NO_x on photochemical smog formation under simulated transport conditions." Envir. Sci. Technol. 17, 58-62.

Duce R.A. (1969) On the source of gaseous chlorine in the marine atmosphere. J. Geophys. Res. 70, 1775-1779.

Glasson W.A. (1981) Effect of hydrocarbons and NO_x on photochemical smog formation under simulated transport conditions. J. Air Pollut. Control Assoc. 31, 1169-1172.

Glasson W.A. (1983) Reply to Comment on "Effect of nitrogen oxide emissions in metropolitan regions," "Effect of NO_x emission rates on smog formation in the California South Coast Air Basin", and "Effect of hydrocarbon and NO_x on photochemical smog formation under simulated transport conditions." Envir. Sci. Technol. 17, 62-63.

Goodin W.R., McRae G.J. and Seinfeld, J.H. (1979) A comparison of interpolation methods for sparse data: Application to wind and concentration fields. J. Appl. Met. 18, 761-771.

Gray H.A., Cass G.R., Huntzicker J.J., Heyerdahl E.K. and Rau J.A. (1985) Characteristics of atmospheric organic and elemental carbon particles in Los Angeles. Envir. Sci. Technol. (submitted).

Grosjean D. and Fung K. (1984) Hydrocarbons and carbonyls in Los Angeles air. J. Air Pollut. Control Assoc. 34, 537-543.

Hildemann L.M., Russell A.G. and Cass G.R. (1984) Ammonia and nitric acid concentrations in equilibrium with atmospheric aerosols: Experiment vs. theory. Atmos. Environ. 18, 1737-1750.

Larson S.M., Cass G.R., Hussey K.J. and Luce F. (1984) Visibility model verification by image processing techniques. Final report to the California Air Resources Board under Agreement A2-077-32, Environmental Quality Laboratory, California Institute of Technology, Pasadena, CA.

Martens C.S., Wesolowski J.J., Harriss R.C. and Kaifer R. (1973) Chlorine loss from Puerto Rican and San Francisco Bay area marine aerosols. J. Geophys. Res. 78, 8778-8792.

Muck R.E. and Steenhuis T.S. (1982) Nitrogen losses from manure storages. Agricultural Wastes 4, 41-54.

Ohgaki H., Matsukura N., Morino K., Kawachi T., Sugimura T., Morita K., Tokima H. and Hirota T. (1982) Carcinogenicity in rats of the mutagenic compounds 1-nitropyrene and 3-nitrofluoroanthene. Cancer Letters 15, 1-7.

Pitts J.N., Winer A.M., Atkinson R. and Carter W.P.L. (1983) Comment on "Effect of nitrogen oxide emissions in metropolitan regions," "Effect of NO_x emission rates on smog formation in the California South Coast Air Basin," and "Effect of hydrocarbon and NO_x on photochemical smog formation under simulated transport conditions." Envir. Sci. Technol. 17, 54-57.

Ranzieri A. (1983) Private communication: forwarded magnetic tape AR3288, "1982-SCAB Point and Area Source Emissions." California Air Resources Board, Sacramento.

Ranzieri A. (1984) Private communication: forwarded magnetic tape AR3292, "1982-SCAB Point and Area Source Emissions." California Air Resources Board, Sacramento.

Russell A.G. (1985) Formation and control of atmospheric aerosol nitrate and nitric acid. Ph.D. thesis, California Institute of Technology, Pasadena.

Russell A.G. and Cass G.R. (1984) Acquisition of regional air quality model validation data for nitrate, sulfate, ammonium ion and their precursors. Atmospheric Environment 18, 1815-1827.

Russell A.G., McRae G.J. and Cass G.R. (1983) Mathematical modeling of the formation and transport of ammonium nitrate aerosol. Atmospheric Environment 17, 949-964.

Russell A.G., McRae G.J. and Cass G.R. (1985) The dynamics of nitric acid production and the fate of nitrogen oxides. Atmospheric Environment 19, 893-903.

South Coast Air Quality Management District and Southern California Association of Governments. (1982) Final Air Quality Management Plan, 1982 Revision.

Spicer C.W. (1983) Smog chamber studies of NO_x transformation rates and nitrate/precursor relationships. Envir. Sci. and Technol. 17, 112-120.

Steenhuis T.S., Bubenzer G.D. and Converse J.C. (1982) Ammonia volatilization of winter spread manure. In Transactions of the American Society of Agricultural Engineers 22, 152-161.

Winer A. M., Peters J.W., Smith J.P. and Pitts J.N. (1974) Response of commercial chemiluminescent NO–NO_2 analyzers to other nitrogen containing compounds. Envir. Sci. Technol. 8, 1118–1121.

TABLE 1

1982 Estimated Emissions within the
Modeling Region Shown in Figure 1

Source Type	Emission Rate		
	THC tons/day	NO_x tons/day	CO tons/day
Stationary Sources			
Fuel Combustion			
External Combustion Boilers			
Utilities	6.7	97.7	8.2
Industrial	3.0	41.0	7.1
Commercial and Institutional	0.1	3.6	0.03
Internal Combustion Engines			
Utilities	4.5	8.4	3.0
Industrial	25.1	58.1	19.2
Petroleum Refining and Production	2.8	35.3	1.1
Other Manufacturing	3.1	39.5	181.3
Residental, Agricultural, and Other	16.9	53.3	127.1
Subtotal Fuel Combustion	62.2	336.9	347.0
Waste Burning and Incineration	0.09	0.4	0.3
Landfill	777.9	0.0	0.0
Solvent Use			
Surface Coating	195.4	1.9	0.4
Other	161.8	0.2	0.03
Petroleum Processes, Storage, and Transfer	99.9	11.3	13.6
Industrial Processes	26.1	2.6	18.1
Miscellaneous	440.0	3.8	118.6
SUBTOTAL STATIONARY SOURCES	1763.4	357.1	498.0
Motor Vehicle Emissions			
On-Road Vehicles	581.4	662.5	5001.9
Off-Road Vehicles	26.8	67.1	172.6
Railroads	3.8	15.3	5.8
Ships	22.2	16.0	88.6
Aircraft	18.1	16.3	84.5
SUBTOTAL MOTOR VEHICLE EMISSIONS	652.3	777.2	5353.4
TOTAL	2415.7	1134.3	5851.4

TABLE 2

Summary of Ammonia Emissions by Source Category
within the Modeling Region Shown in Figure 1

SOURCE CATEGORY	TOTAL EMISSIONS (tons/day)	
Stationary Fuel Combustion		
Electric Utility		
Natural Gas	1.2	
Residual Oil	0.38	
Digester Gas	0.00	
Refinery Fuel Burning		
Natural Gas	0.12	
Residual Oil	0.015	
Refinery Gas	0.39	
Industrial Fuel Burning		
Natural Gas	0.47	
Liquified Petroleum gas (LPG)	0.008	
Residual Oil	0.022	
Distillate Oil	0.12	
Digester Gas	0.026	
Coke Oven Gas	0.015	
Residential/Commercial Fuel Burning		
Natural Gas	0.21	
Liquid Propane Gas (LPG)	0.004	
Residual Oil	0.085	
Distillate Oil	0.079	
Coal	0.023	
Subtotals	3.2	(1.9%)
Mobile Source Fuel Combustion		
Automobiles		
Catalyst Autos and Light Trucks	2.4	
Non-catalyst Autos and Light Trucks	0.48	
Diesel Autos and Light Trucks	0.004	
Catalyst Medium Vehicles	0.23	
Non-catalyst Medium and Heavy Trucks	0.14	
Diesel Trucks	0.023	
LPG for Carburetion	0.007	
Civilian Aircraft		
Jet	0.007	
Piston	0.002	
Shipping		
Residual Oil Boilers	0.068	
Diesel Ships	0.002	
Railroad—Diesel Oil	0.004	
Military		
Gasoline	0.005	
Diesel	0.002	
Jet Fuel	0.002	
Residual Oil	0.001	
Off-Highway Vehicles	0.006	
Subtotals	3.4	(2.0%)
Industrial Point Sources	2.4	(1.5%)
Sewage Treatment Plants	14.6	(8.9%)
Soil Surface	23.8	(14.5%)
Fertilizer		
Farm Crop	2.0	
Orchards	1.6	
Handling	0.4	
Non-farm	4.8	
Subtotals	8.8	(5.4%)
Livestock		
Cattle		
Dairy	29.8	
Feedlot	7.2	
Range	13.6	
Horses	16.2	
Sheep	0.86	
Hogs	0.26	
Chickens	16.4	
Turkeys	0.49	
Subtotals	84.8	(51.6%)
Domestic		
Dogs	11.6	
Cats	3.5	
Human Respiration	0.046	
Human Perspiration	7.6	
Household Ammonia Use	0.57	
Subtotals	23.3	(14.2%)
*** TOTAL ***	164.3	(100%)

TABLE 3

Splitting Factors for Converting Total Measured Hydrocarbons (ppmC) into Hydrocarbon Classes for Use as Initial Conditions

Class	Factor
HCHO	0.0037
RCHO	0.0033
OLE	0.0042
ALK	0.0675
ARO	0.0177
C2H4	0.0061

For example, the initial HCHO concentration = 0.0037 X THC measured in ppmC. The splitting factors above incorporate the conversion from total hydrocarbons given in ppmC to molecular concentrations in ppmV.

TABLE 4

Predicted and measured concentrations along the trajectory beginning at Long Beach, California, at 1100 (PDT) 31 August 1982.

	1400 PDT			1800 PDT			
Pollutant	Measured Concentration	Case 1 Predicted NH_4NO_3 Only	Case 2 Predicted Reaction 58 Included	Measured at Rubidoux	Measured at UCR	Case 1 Predicted NH_4NO_3 Only	Case 2 Predicted Reaction 58 Included
O_3 (ppb)	173[3]	174	174	130	150	152	152
NO_2 (ppb)	70[3]	51[1]	52[1]	50	-	35[1]	38[1]
HNO_3 (ppb)	10.1-7.7[2]	10.0	8.2	5.3-1.8[2]	2.0	3.3	2.5
AN ($\mu g\ m^{-3} NO_3^-$)	7.6-13.4[2]	11.6	19.9	29.7-14.4[2]	21.9	14.1	22.7
TN ($\mu g\ m^{-3} NO_3^-$)	33.0-32.8[2]	36.8	40.6	43.1-18.9[2]	27.0	22.4	29.0
NH_3 (ppb)	15.3-10.9[2]	10.8	13.2	59.8-89.0[2]	32.7	27.3	36.4
PAN (ppb)	*	*	*	*	22	20.1	20.1
NH_4NO_3 ($\mu g\ m^{-3} NO_3^-$)		11.6	6.1			14.1	11.3
BAN[4] ($\mu g\ m^{-3} NO_3^-$)			13.9				11.3

NOTES:

(1) Predicted NO_2 concentrations are the sum of predicted NO_2, HNO_3, AN, and PAN. The instruments used to measure NO_2 possess a quantitative interference due to co-pollutant species (Winer et al., 1974)

(2) Both at Anaheim and at Rubidoux, the trajectory passed nearby between two sampling periods. Both the measured concentrations from 1200 to 1400 and 1400 to 1600 are shown, respectively, at Anaheim. Likewise at Rubidoux the measured concentrations for 1600 to 1800 and 1800 to 2000 are given. The UCR site sampling interval was from 1700 to 1900. Predicted ozone values are one-hour averages, as are the measured concentrations.

(3) Ozone and NO_2 concentrations are averaged values from the nearest three stations. Other concentrations are for Anaheim.

(4) Bound Aerosol Nitrate

(*) PAN measured only at UCR.

TABLE 5
Effect of Emission Reductions on Nitrate Species Concentrations
Rubidoux, CA, 31 August 1982

Aerosol Nitrate
Maximum Two-Hour Average
($\mu g\ m^{-3}$)

	Base Case THC					THC Emissions Reduced 30%	
	NO_x Emissions Reduction					NO_x Emissions Reduction	
	0%	20%	40%	60%	80%	0%	20%
Base Case NH_3 Emissions	27.0	16.3	11.7	8.3	3.4	31.2	19.5
Reduced NH_3 Emissions	7.2	6.4	–	–	–	7.0	6.3

Aerosol Nitrate
24-hour Average
($\mu g\ m^{-3}$)

	Base Case THC					THC Emissions Reduced 30%	
	NO_x Emissions Reduction					NO_x Emissions Reduction	
	0%	20%	40%	60%	80%	0%	20%
Base Case NH_3 Emissions	11.5	8.4	4.8	2.7	1.1	13.3	9.0
Reduced NH_3 Emissions	2.8	1.8	–	–	–	2.8	1.8

Total Nitrate
24-hour Average
($\mu g\ m^{-3}$)

	Base Case THC					THC Emissions Reduced 30%	
	NO_x Emissions Reduction					NO_x Emissions Reduction	
	0%	20%	40%	60%	80%	0%	20%
Base Case NH_3 Emissions	18.6	15.4	10.3	6.8	4.0	21.2	15.9
Reduced NH_3 Emissions	16.1	13.1	–	–	–	16.9	13.1

Nitric Acid
Maximum Two-Hour Average
(ppb)

	Base Case THC					THC Emissions Reduced 30%	
	NO_x Emissions Reduction					NO_x Emissions Reduction	
	0%	20%	40%	60%	80%	0%	20%
Base Case NH_3 Emissions	9.6	7.9	5.9	4.1	2.6	10.1	8.0
Reduced NH_3 Emissions	16.9	13.2	–	–	–	18.8	14.2

TABLE 6

Predicted Peak One-Hour Ozone Concentrations (ppb) at Rubidoux as a Function of Emission Reductions 31 August 1982

	NO_x Emission Reduction				
	0%	20%	40%	60%	80%
% THC Reduction					
0%*	190	170	144	117	80
30%	181	166	(a)	(a)	(a)

*0% = base case

(a) not examined

TABLE 7

Predicted Pollutant Concentrations
at Rubidoux, California
when Emissions of SINK aerosol are Included

	AN Max 2-Hr Avg ($\mu g\ m^{-3}$)	AN 24-Hr Avg ($\mu g\ m^{-3}$)	TN 24-Hr Avg ($\mu g\ m^{-3}$)	HNO_3 (g) Max 2 Hr (ppb)
Base Case, No SINK	27.0	11.5	18.6	9.6
Base Case, SINK Included	29.4	13.8	21.4	9.3
SINK Included, NH_3 Emissions Reduced	14.4	8.3	18.9	12.7

Figure Captions

Figure 1. Gridded map of California's South Coast Air Basin (SoCAB) used for constructing concentration fields, meteorological fields, and emissions inventories. Symbols (•) indicate the locations of aerosol measurement stations used in this work. The solid line marks the boundary of the SoCAB.

Figure 2. Spatial distribution of the 1982 estimated daily emissions of NH_3, NO_x, THC and CO in the South Coast Air Basin.

Figure 3. Observed and predicted O_3 at Rubidoux, CA, 31 August 1982.

Figure 4. Observed and predicted NO_2 at Rubidoux, CA, 31 August 1982.

Figure 5. Observed and predicted Total Nitrate (TN = AN + HNO_3) at Rubidoux, CA, 31 August 1982.

Figure 6. Observed and predicted $HNO_3(g)$ at Rubidoux, CA, 31 August 1982.

Figure 7. Observed and predicted NO_3^- at Rubidoux, CA, 31 August 1982.

Figure 8. Observed and predicted NH_3 at Rubidoux, CA, 31 August 1982.

Figure 9. Observed and predicted NO_3^- at Rubidoux, CA, 31 August 1982 when the partition of computed TN between $HNO_3(g)$ and aerosol nitrate is based on ambient temperatures and ammonia concentrations measured at the Rubidoux monitoring site.

Figure 10. Predicted Total Nitrate (TN = $HNO_3(g)$ + NH_4NO_3 + BAN), Aerosol Nitrate (AN = NH_4NO_3 + BAN) and aerosol nitrate formed by reaction 58 (BAN, see text) at Rubidoux, CA, 31 August 1982.

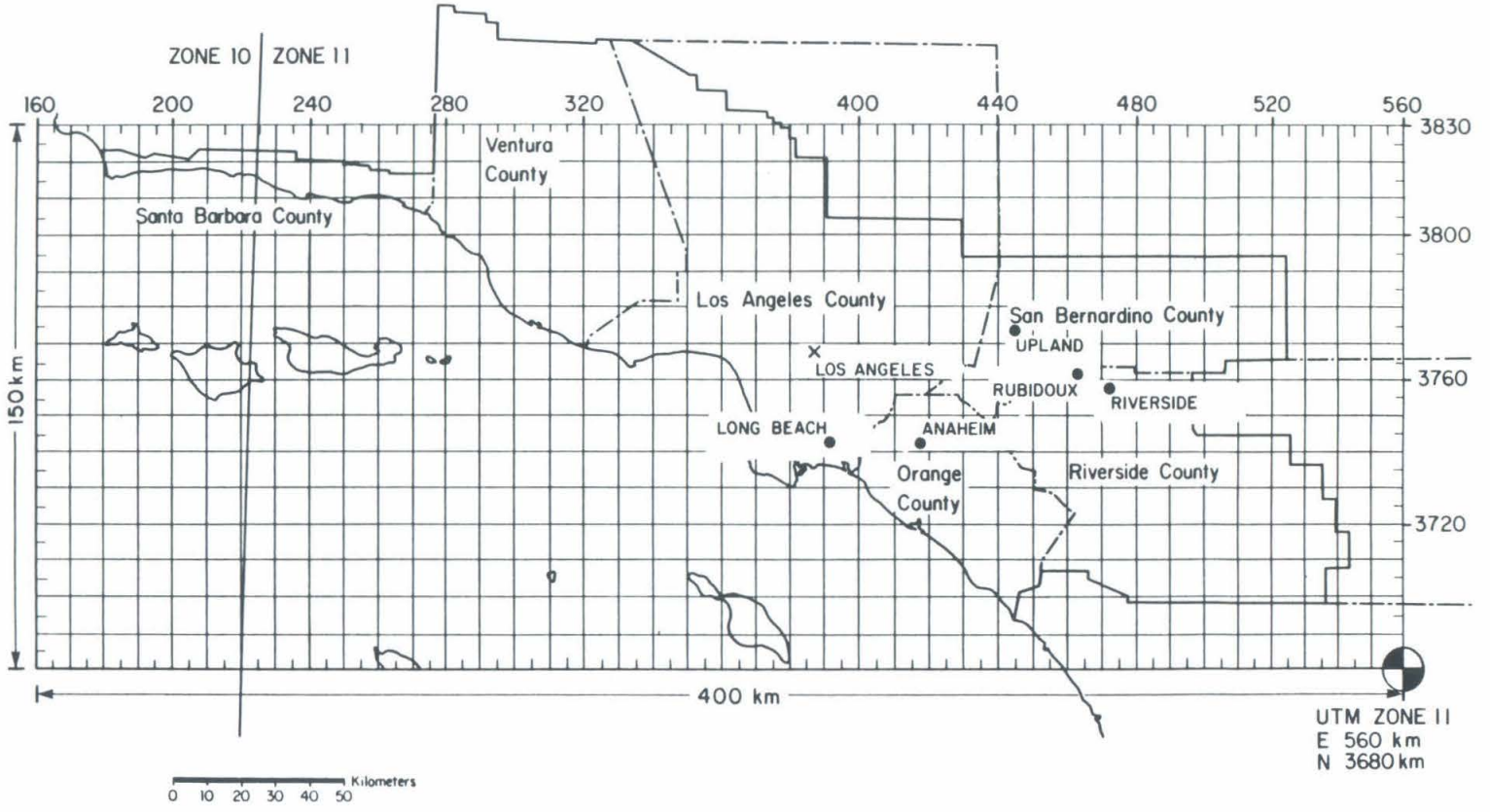

FIGURE 1

Gridded map of California's South Coast Air Basin (SoCAB) used for constructing concentration fields, meteorological fields, and emissions inventories. Symbols (•) indicate the locations of aerosol measurement stations used in this work. The solid line marks the boundary of the SoCAB.

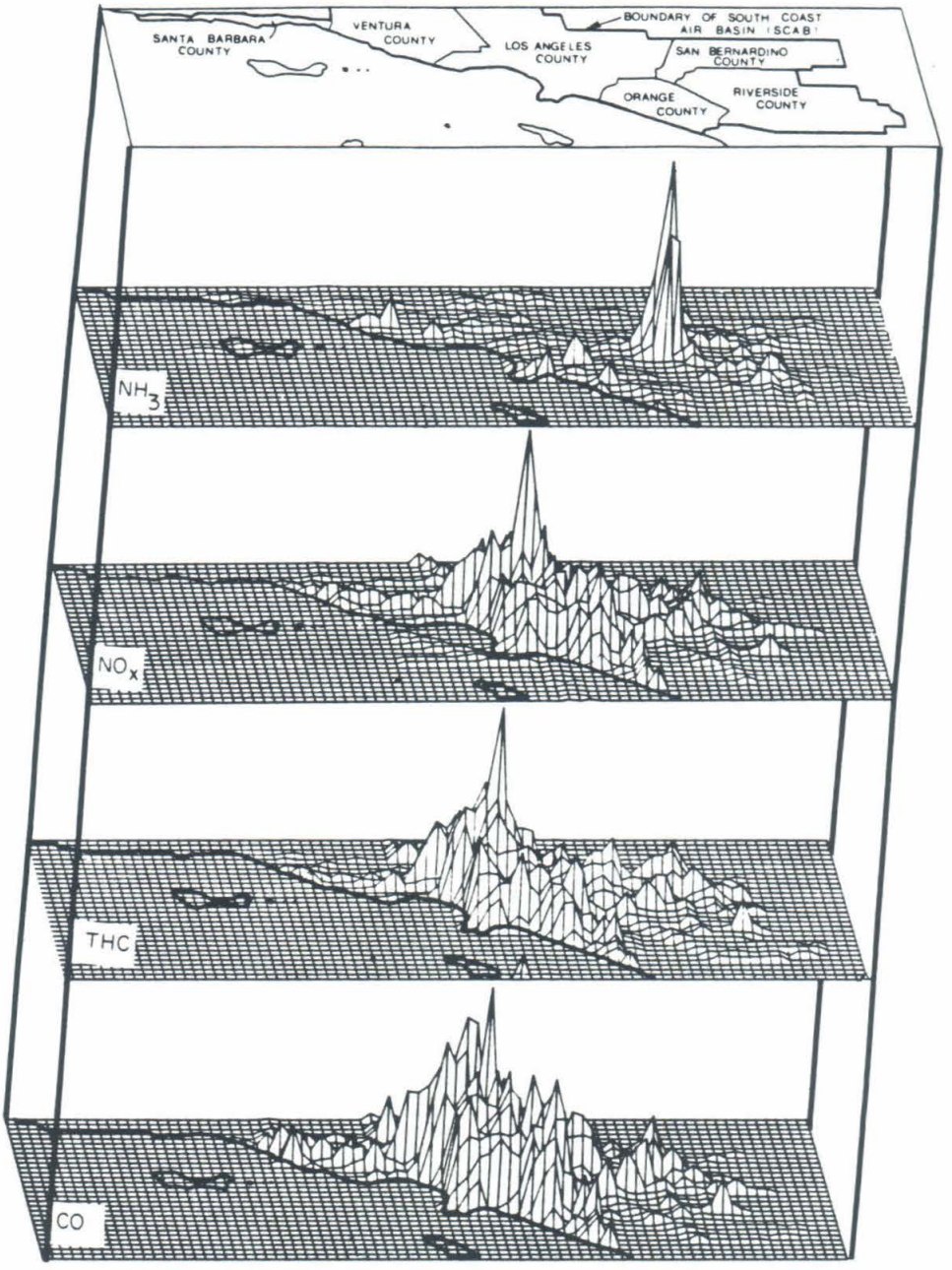

FIGURE 2

Spatial distribution of the 1982 estimated daily emissions of NH_3, NO_x, THC, and CO in the South Coast Air Basin.

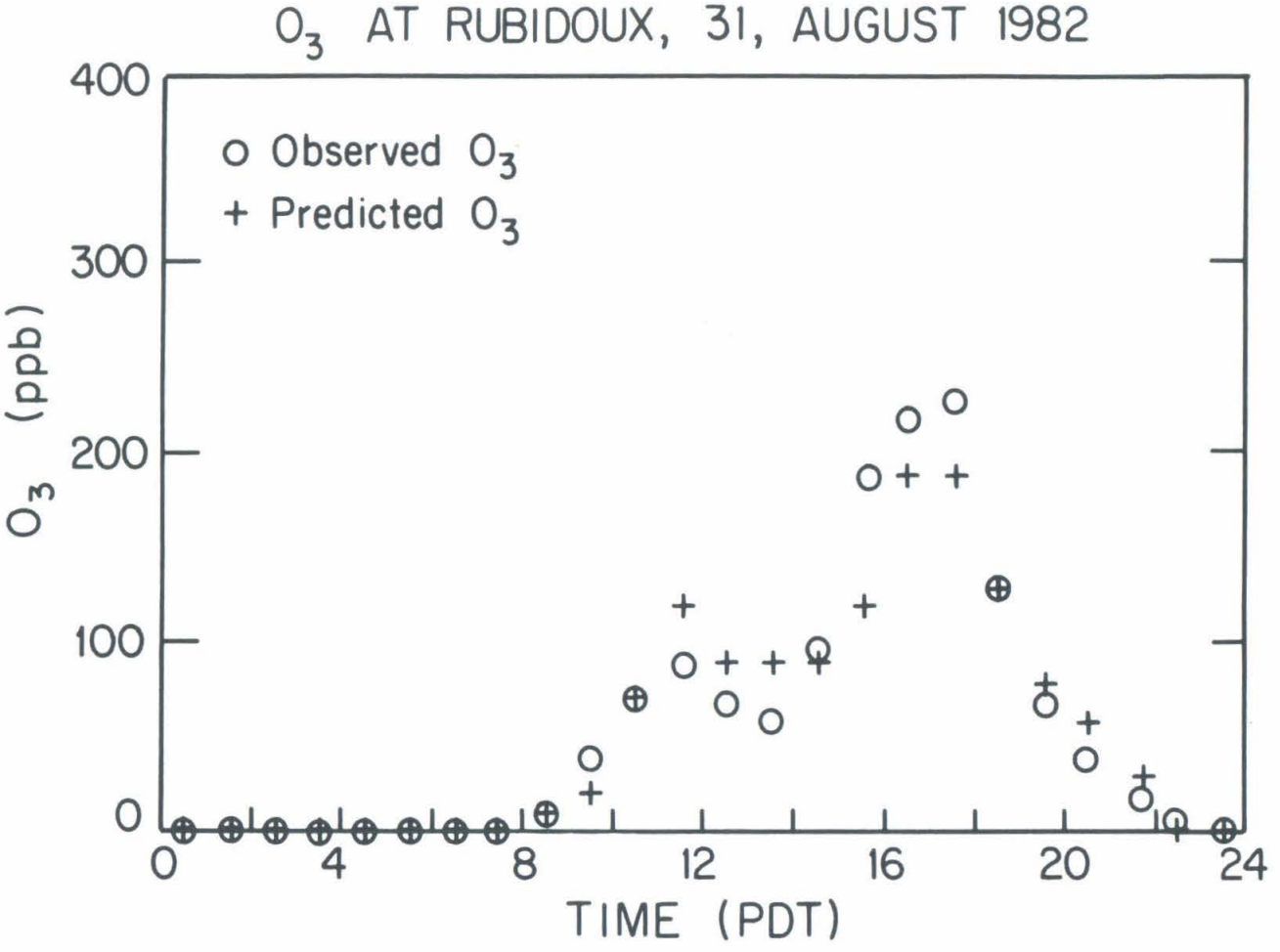

FIGURE 3

Observed and predicted O_3 at Rubidoux, CA, 31 August 1982.

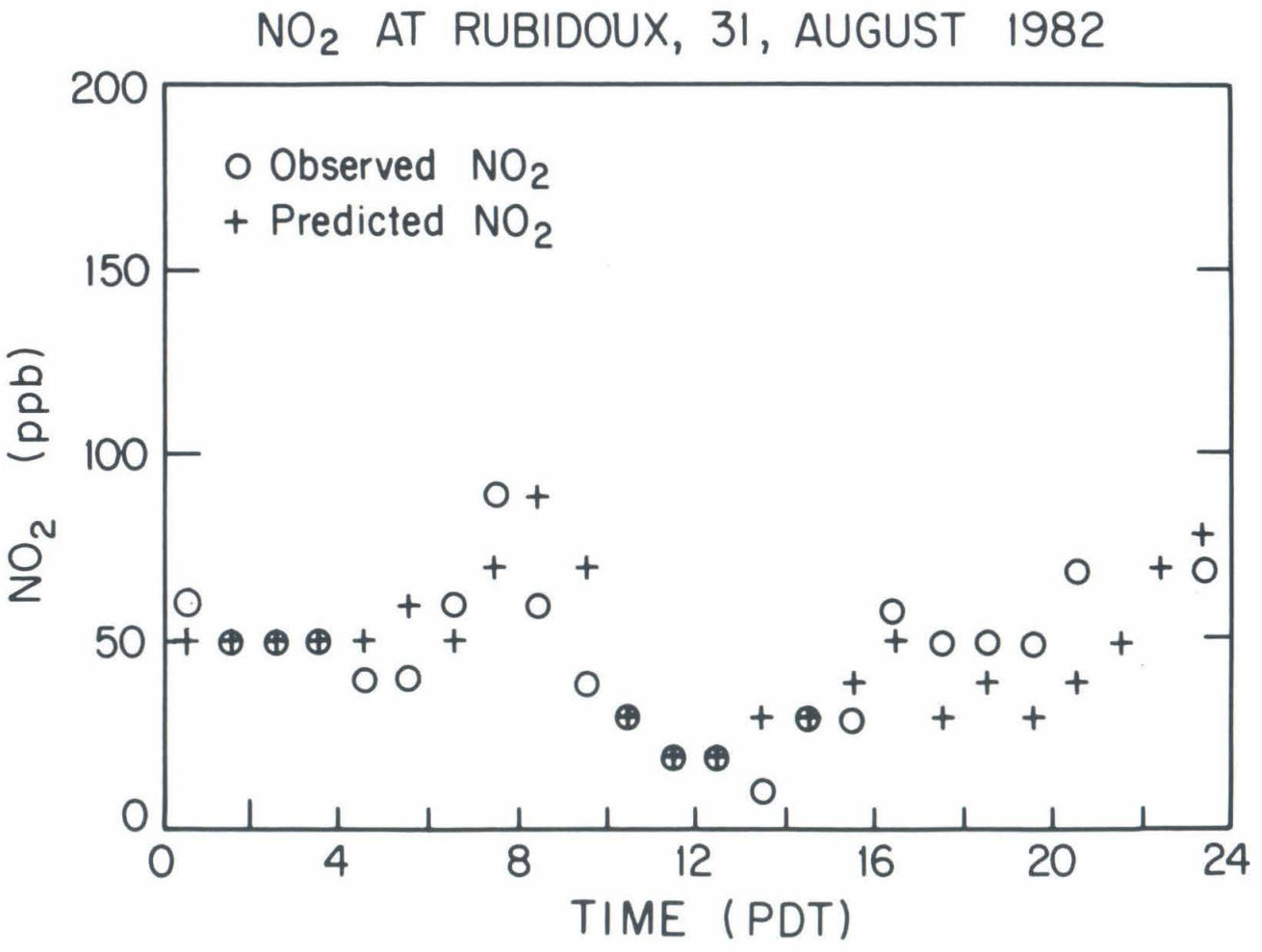

FIGURE 4

Observed and predicted NO_2 at Rubidoux, CA, 31 August 1982.

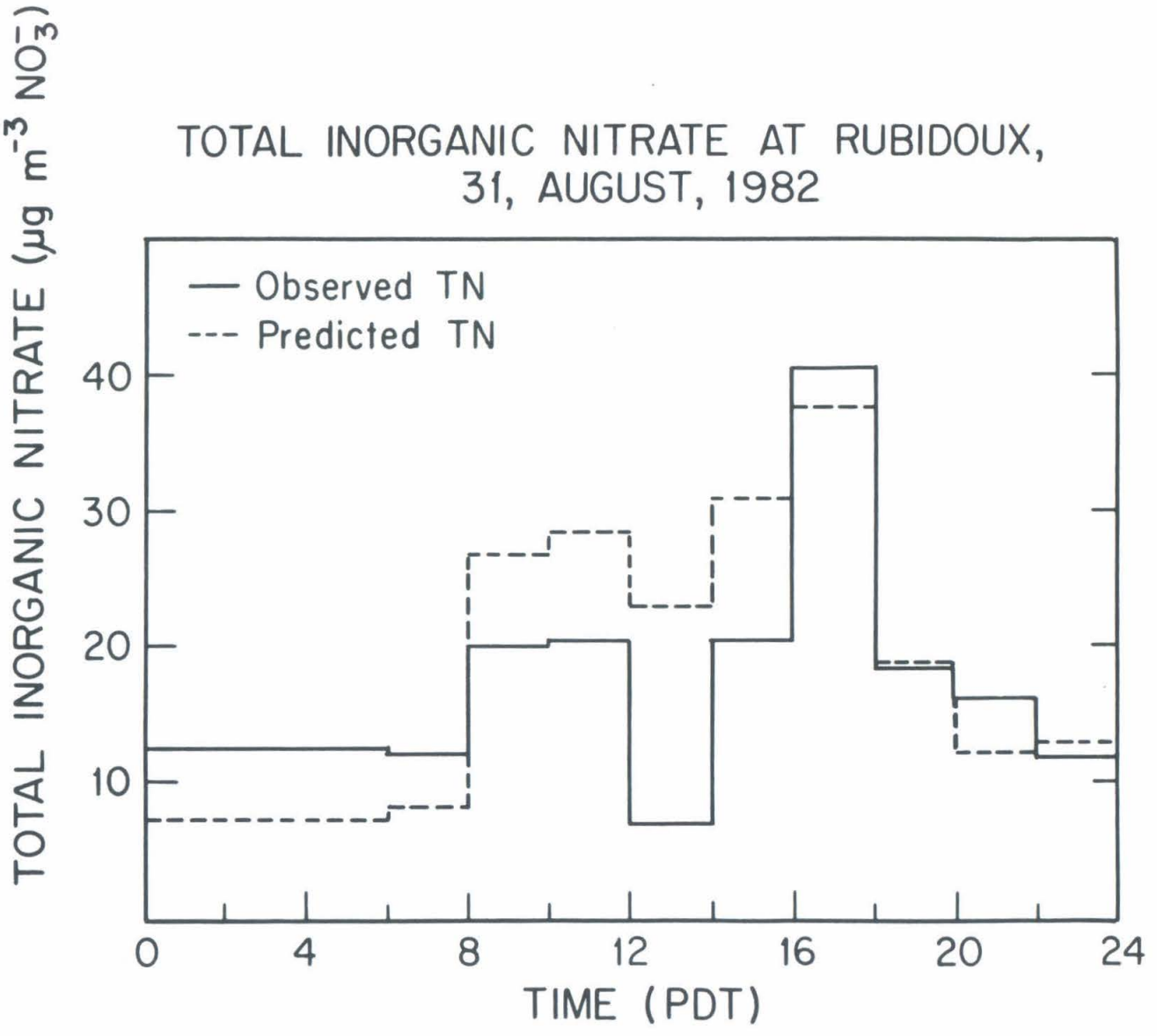

FIGURE 5

Observed and predicted Total Nitrate (TN = AN + HNO_3) at Rubidoux, CA, 31 August 1982.

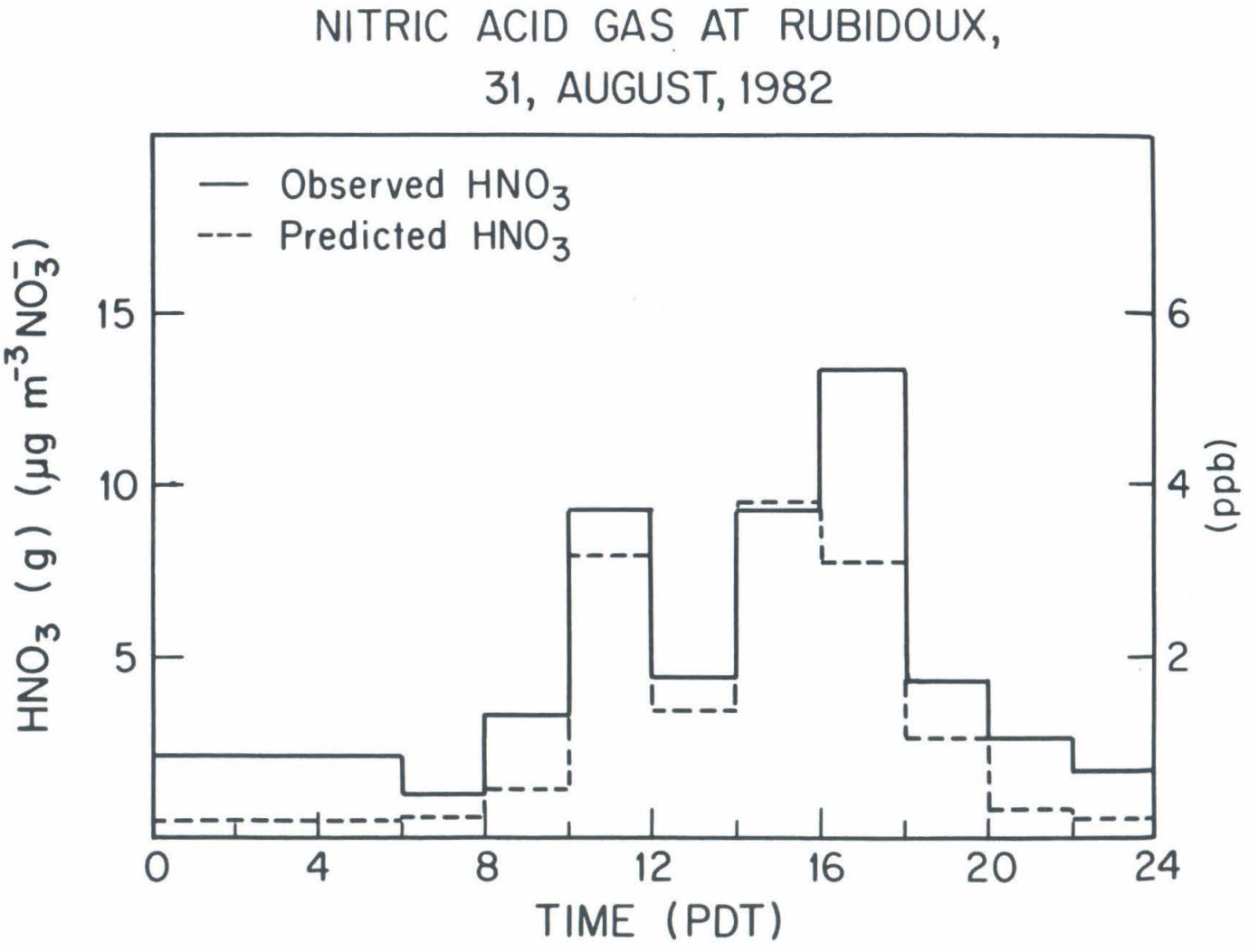

FIGURE 6

Observed and predicted HNO_3 (g) at Rubidoux, CA, 31 August 1982.

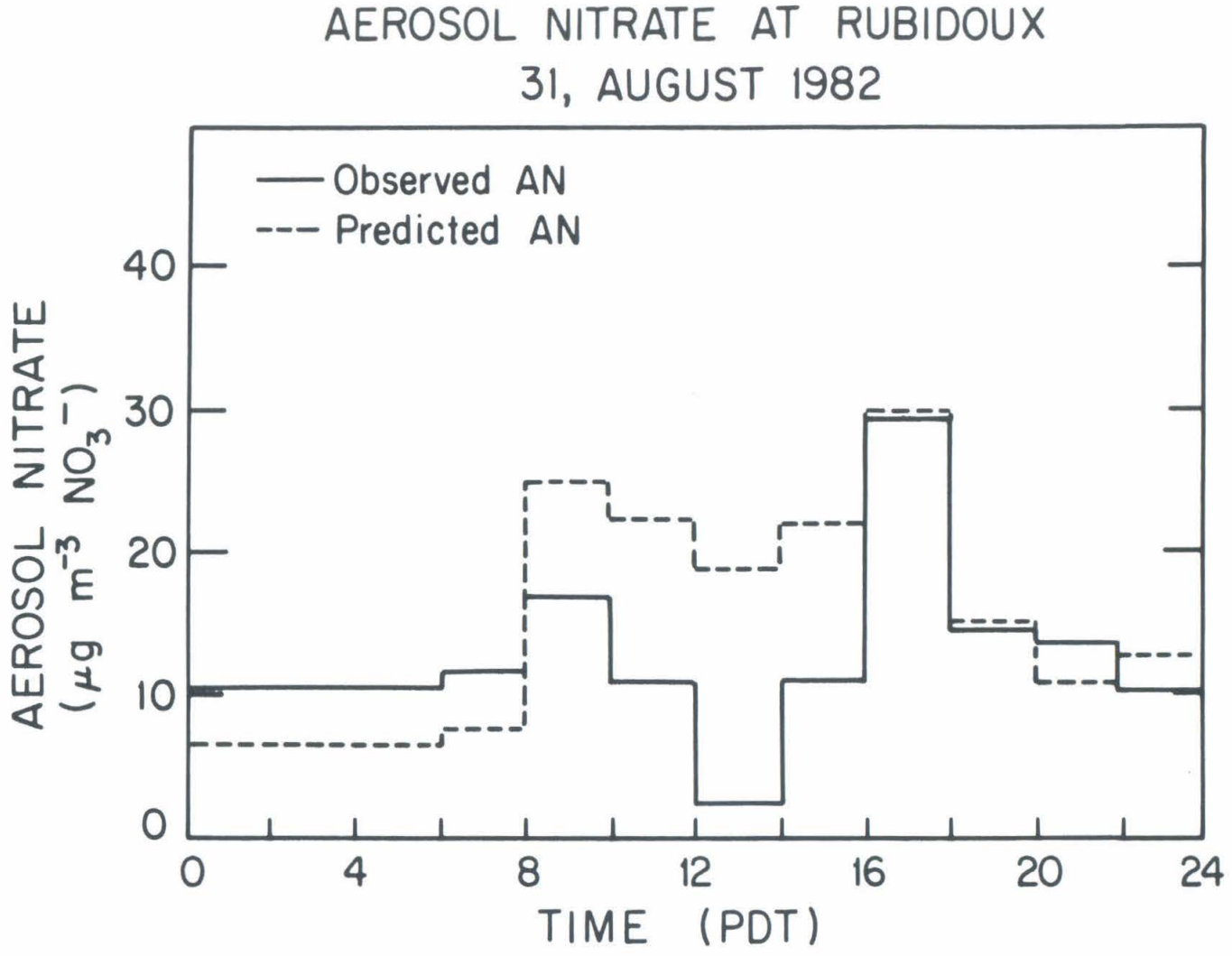

FIGURE 7
Observed and predicted NO_3^- at Rubidoux, CA, 31 August 1982.

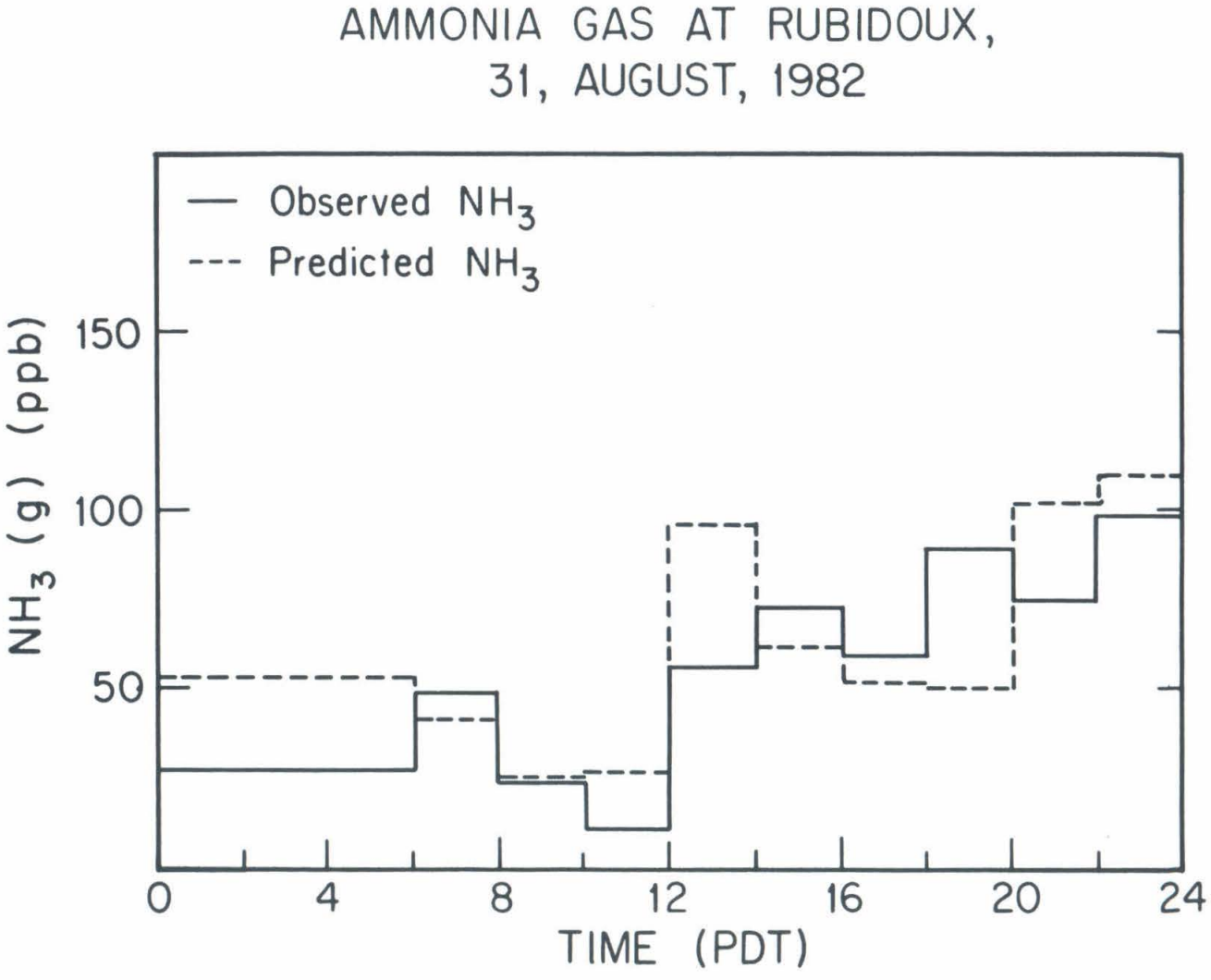

FIGURE 8

Observed and predicted NH_3 at Rubidoux, CA, 31 August 1982.

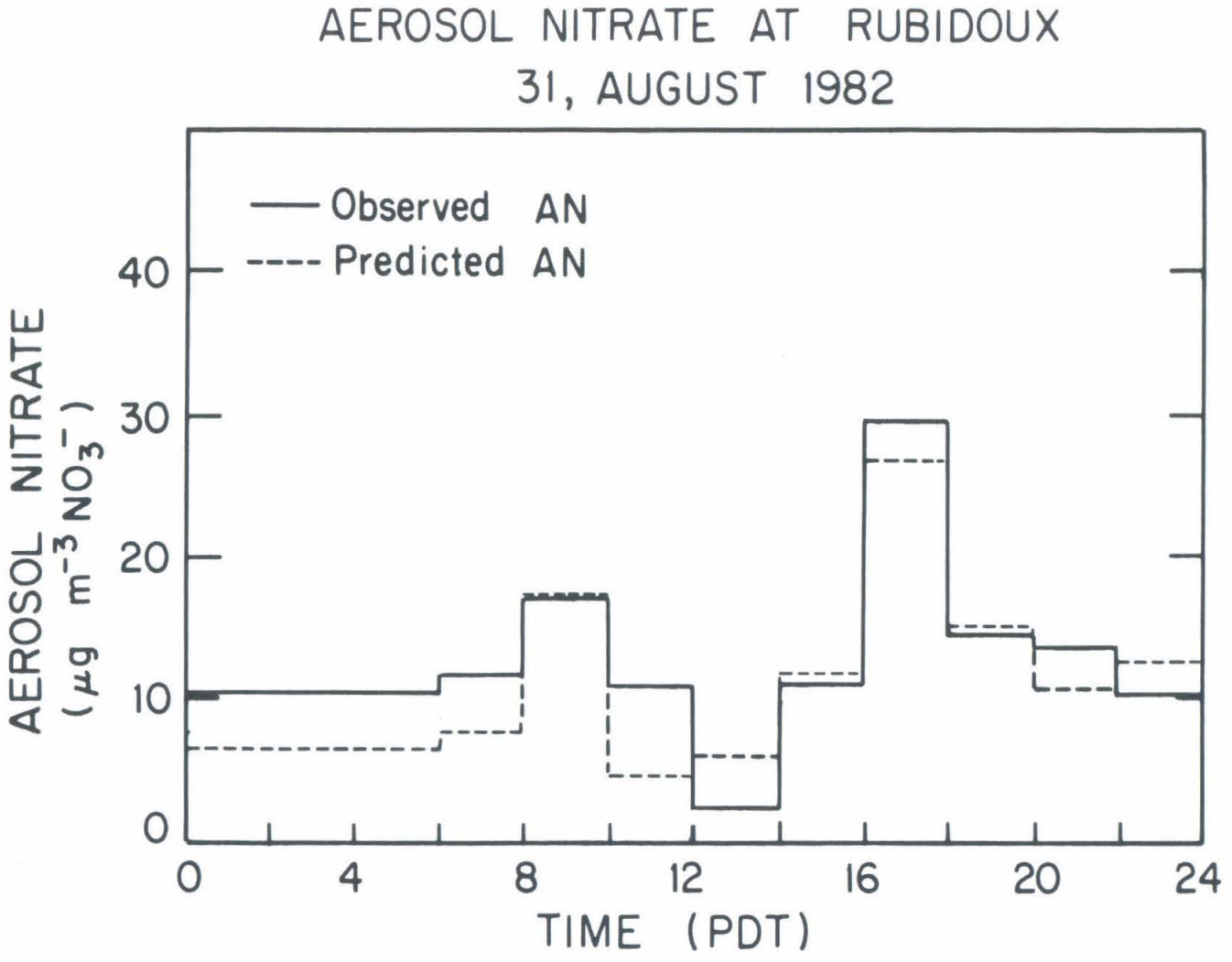

Figure 9

Observed and predicted NO_3^- at Rubidoux, CA, 31 August 1982 when the partition of computed TN between $HNO_3(g)$ and aerosol nitrate is based on ambient temperatures and ammonia concentrations measured at the Rubidoux monitoring site.

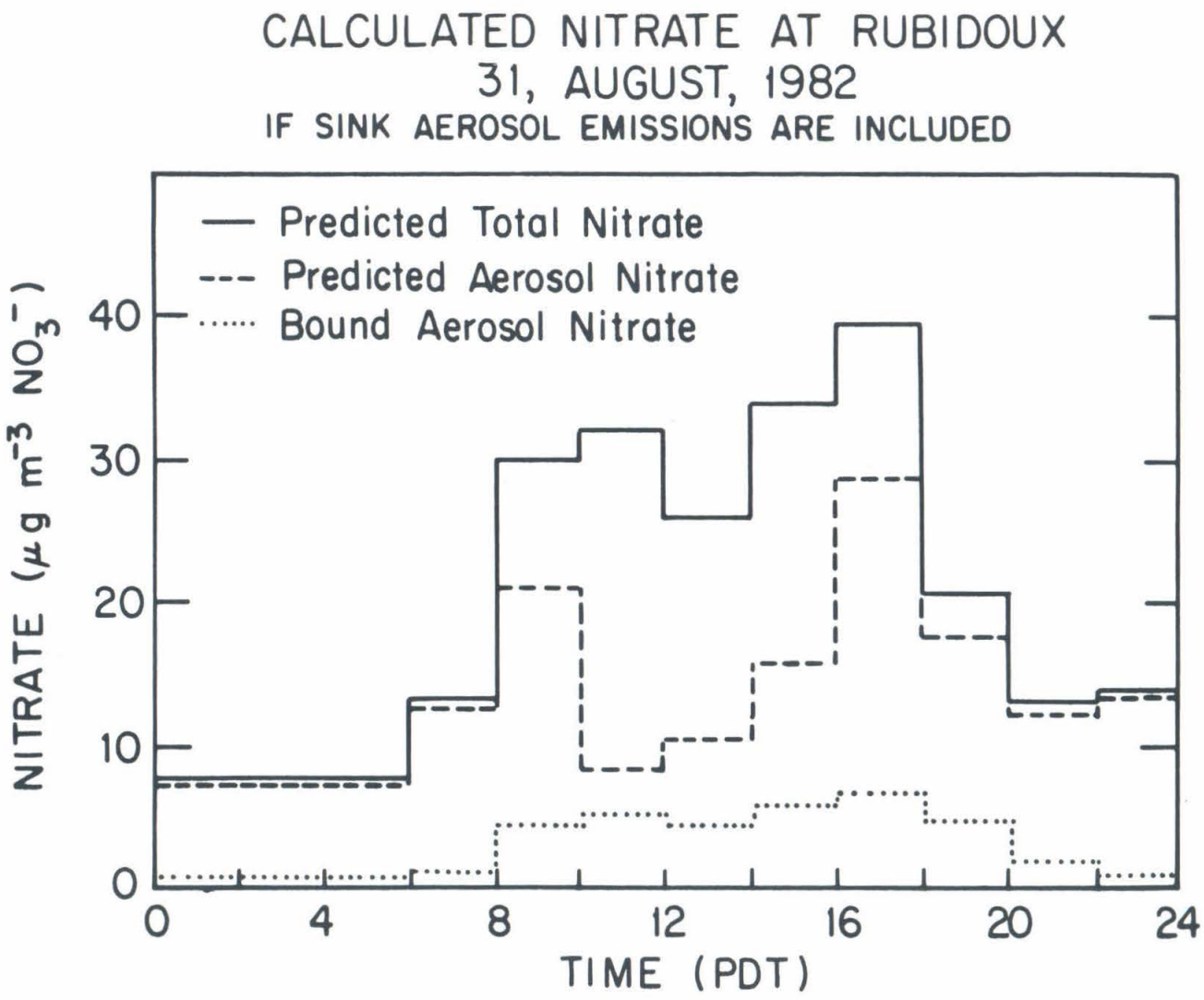

FIGURE 10

Predicted Total Nitrate (TN = $HNO_3(g)$ + NH_4NO_3 + BAN), Aerosol Nitrate (AN = NH_4NO_3 + BAN) and aerosol nitrate formed by reaction 58 (BAN, see text) at Rubidoux, CA, 31 August 1982.